p28

DEPARTMENT OF AEROSPACE ENGINEERING
COLLEGE OF ENGINEERING AND TECHNOLOGY
OLD DOMINION UNIVERSITY
NORFOLK, VA 23529-0247

PANEL FLUTTER AND SONIC FATIGUE ANALYSIS FOR RLV

By
Dr. Chuh Mei, Principal Investigator
Guangfeng Cheng, Graduate Research Assistant
Department of Aerospace Engineering

FINAL REPORT
For the period ending December 31, 2000

Prepared for
NASA Langley Research Center
Attn: Dr. Max L. Blosser
Technical Monitor
Mail Stop 396
Hampton, VA 23681-0001

Under
NASA Research Grant NAG-1-2150
ODURF File No. 191881

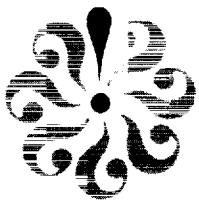

May 2001

ABSTRACT

Panel Flutter and Sonic Fatigue Analysis for RLV

Chuh Mei and Guangfeng Cheng
Department of Aerospace Engineering
Old Dominion University, Norfolk, Virginia 23529-0247

A methodology is presented for the flutter analysis of the seal of thermal protection system (TPS) panel of X-33 Advanced Technology Demonstrator test vehicle. The seal is simulated as a two-dimensional cantilevered panel with an elastic stopper, which is modeled as an equivalent spring. This cantilever beam-spring model under the aerodynamic pressure at supersonic speeds turns out to be an impact nonlinear dynamic system. The flutter analysis of the seal is thus carried out using time domain numerical simulation with a displacement stability criterion. The flutter boundary of the seal is further verified with a family of three traditional and one nontraditional panel flutter models. The frequency domain method that applies eigenanalysis on the traditional panel flutter problem was used. The results showed that the critical dynamic pressure could be more than doubled with properly chosen material for the base stopper. The proposed methodology can be easily extended to three-dimensional panel seals with flow angularity.

FOREWORD

This technical report contains the research results on supersonic panel flutter analysis of thermal protection system (TPS) seals. The research is sponsored by a NASA Langley Research Center Grant NAG-1-2150, entitled "Panel Flutter and Sonic Fatigue Analysis for RLV." Technical monitor is Dr. Max L. Blosser, Metal and Composite Thermal Structures Branch, NASA Langley Research Center. Two journal publications have resulted from this research grant: (1)"Nonlinear Response of Composite Panels Under Combined Acoustic Excitation and Aerodynamic Pressure," AIAA Journal, Vol. 38, No. 9, 2000, pp.1534-1542. and (2)"A Methodology for Supersonic Panel Flutter Analysis of TPS Seals," accepted for publication and to appear in Journal of Aircraft, July 2001. The authors are extremely thankful to Max Blosser for many technical discussions and suggestions.

TABLE OF CONTENTS

NOMENCLATURE

$[a_a]$, $[A_a]$	= element and system aerodynamic influence matrices
b	= beam width
C_a	= aerodynamic damping coefficient
$\{d\}$	= element nodal displacement vector
E	= Young's modulus
F_e	= impact force
g_a	= non-dimensional aerodynamic damping
$[g]$, $[G]$	= element and system aerodynamic damping matrices
h	= beam thickness
I	= area moment of inertia
k_s	= equivalent spring stiffness
$[K_e]$, $[K]$	= element and system stiffness matrices
L	= beam length
M	= Mach number
$[m]$, $[M]$	= element and system mass matrices
$\lfloor N \rfloor$	= beam element shape functions
P_a	= aerodynamic pressure
q	= dynamic pressure
$\{Q_e\}$, $\{Q\}$	= element and system load vectors
V	= airflow speed
w	= transverse displacement
W_e	= transverse deflection at beam free end
$\{W\}$	= system nodal displacement vector
α	= panel damping rate
κ	= non-dimensional eigenvalue
λ	= non-dimensional dynamic pressure
μ	= mass ratio
ρ, ρ_a	= beam and air mass densities
$\{\Phi\}$	= eigenvector
ω, ω_o	= panel and reference frequencies
Ω	= complex panel motion parameter

INTRODUCTION

Various methods have been employed to solve the panel flutter[1,2] problem, which is among the general considerations for designing structures under supersonic/hypersonic conditions. In point of dynamics, the flutter boundary generally takes the form of critical non-dimensional dynamic pressure. The solution means can be classified in two categories:[3] frequency domain methods and time domain methods. While using finite element analysis, frequency domain methods are feasible while the problem can be cast as an eigenvalue problem. However, when it's mathematically difficult to execute eigenanalysis, time domain methods can be applied for determining flutter. The acceptability of the results depends on the numerical stability of the methods adopted.

The problem cited in this paper arises from the stability analysis of the seal of superalloy honeycomb thermal protection system (TPS) panel of X-33 vehicle.[4] From the blueprint of the seal for two adjacent TPS panels, a sketch was made and shown in Fig. 1. The vibration of the covering seal is restrained with the neighboring panel. As the overhead airflow speed increased, flutter will occur. The seal is restrained to move downward by the top surface of the adjacent panel and a tiny gap (or zero gap) exists between the seal and the adjacent panel. Therefore, a simplified two-dimension model for the seal (flow angle $\Lambda = 0^0$) is idealized as a cantilever beam with a stopper below its free end, as shown in Fig. 2. Accordingly, the problem turns out to be a vibration problem with an impact at some amplitude.

If the stopper is very stiff so that it can be taken as a rigid stopper, the beam will undergo impact force during its vibration and a restitution coefficient can be included to allow for energy loss. [5] However, the stopper should be treated as elastic, then more

considerations are needed. For this case, an equivalent spring can be used to replace the stopper. In investigation of the family of beams with left end clamped, right end using various supports as shown in Fig. 3, flutter analysis of the spring stopper model as well as the bar stopper model, which is closer to real flutter problem, belongs to nontraditional panel flutter analysis. In the present paper, time domain method is developed and employed to solve this nontraditional flutter problem. Apparently, flutter of model I, model IV and model V in Fig. 3 is traditional panel flutter since eigenanalysis is applicable.

The systematic procedures of finite element analysis were followed, considering the aerodynamic effect with quasi-steady first-order piston theory. For the spring stopper model, the equivalent spring stiffness is from the assumption that the stopper undergoes elastic deformation. Thus, the impact force is the restitution force of the equivalent spring. Main interest is focused on the variation of critical dynamic pressure versus stopper stiffness. The flutter boundary is compared with those of similar cases with simpler boundary conditions.

FINITE ELEMENT FORMULATION

The classical Euler-Bernoulli beam element can be extended with consideration of aerodynamic effects: additional aerodynamic damping and influence matrices need to be derived. The equations of motion (EOM) which govern the motion of the beam are derived from the principle of virtual work.

Element Matrices and System Equations of Motion

From the quasi-steady first-order piston theory, the aerodynamic pressure applied on the beam is

$$P_a = -\frac{2q}{\sqrt{M_\infty^2 - 1}}\left(w_{,x} + \frac{M_\infty^2 - 2}{M_\infty^2 - 1}\frac{1}{V}w_{,t}\right) \tag{1}$$

or

$$P_a = -\left(\lambda \frac{EI}{bL^3} w_{,x} + \frac{g_a EI}{b\omega_0 L^4} w_{,t}\right) \tag{2}$$

where $q = \rho_a V^2/2$ is the dynamic pressure, V is the airflow speed, ρ_a is the air density, M_∞ is the Mach number, and E, I, b, L are property parameters of the beam. The non-dimensional dynamic pressure and aerodynamic damping coefficient are given by

$$\lambda = \frac{2qL^3 b}{EI\sqrt{M_\infty^2 - 1}} \tag{3}$$

$$g_a = \frac{\rho_a V(M_\infty^2 - 2)}{\rho h \omega_0 (M_\infty^2 - 1)^{3/2}} \approx \sqrt{\lambda C_a} \tag{4}$$

where ρ is the mass density of the beam, $\omega_0 = (EI/\rho AL^4)^{1/2}$ is the reference frequency and C_a is aerodynamic damping coefficient ($C_a \approx \mu/M_\infty$ for $M_\infty >> 1$, and $\mu = \rho_a L/\rho h$ is the mass ratio).

For Euler-Bernoulli element

$$w = \lfloor \mathbf{N}_1\ \mathbf{N}_2\ \mathbf{N}_3\ \mathbf{N}_4 \rfloor \left(w_1\ w_{,x1}\ w_2\ w_{,x2}\right)^T = \lfloor \mathbf{N} \rfloor \{\mathbf{d}\} \tag{5}$$

thus, we have

$$w_{,x} = \frac{\partial w}{\partial x} = \lfloor \mathbf{N} \rfloor_{,x} \{\mathbf{d}\} \qquad w_{,xx} = \frac{\partial^2 w}{\partial x^2} = \lfloor \mathbf{N} \rfloor_{,xx} \{\mathbf{d}\}$$

$$w_{,t} = \lfloor \mathbf{N} \rfloor \{\dot{\mathbf{d}}\} \qquad w_{,tt} = \lfloor \mathbf{N} \rfloor \{\ddot{\mathbf{d}}\} \tag{6}$$

The strain energy of beam element is

$$U_e = \frac{1}{2}\int_0^{h_e} EI(w_{,xx})^2 \mathrm{d}x$$

where h_e is element length. Using Eqs. (6), the variation of strain energy can be expressed as

$$\delta U_e = \{\delta \mathbf{d}\}^T EI \int_0^{h_e} \lfloor \mathbf{N} \rfloor_{,xx}^T \lfloor \mathbf{N} \rfloor_{,xx} \mathrm{d}x \{\mathbf{d}\} \tag{7}$$

Similarly the virtual work done by external forces is

$$\delta W_e = \iint_A \delta v(P_a - \rho h w_{,tt})\mathrm{d}A + \delta w F_e - \{\delta \mathbf{d}\}^T \frac{g_a}{\omega_0}\frac{EI}{L^4}\int_0^{h_e} \lfloor \mathbf{N} \rfloor^T \lfloor \mathbf{N} \rfloor \mathrm{d}x \{\dot{\mathbf{d}}\}$$

$$- \{\delta \mathbf{d}\}^T \frac{1}{\omega_0}\frac{EI}{\rho A L^4}\rho h b \int_0^{h_e} \lfloor \mathbf{N} \rfloor^T \lfloor \mathbf{N} \rfloor \mathrm{d}x \{\ddot{\mathbf{d}}\} + \{\delta \mathbf{d}\}^T \lfloor \mathbf{N} \rfloor^T \{\mathbf{F}_e\} \tag{8}$$

Use the principle of virtual work $\delta U_e = \delta W_e$

$$\{\delta \mathbf{d}\}^T \frac{1}{\omega_0^2}\frac{EI}{L^4}\int_0^{h_e} \lfloor \mathbf{N} \rfloor^T \lfloor \mathbf{N} \rfloor \mathrm{d}x \{\ddot{\mathbf{d}}\} + \{\delta \mathbf{d}\}^T \frac{g_a}{\omega_0}\frac{EI}{L^4}\int_0^{h_e} \lfloor \mathbf{N} \rfloor^T \lfloor \mathbf{N} \rfloor \mathrm{d}x \{\dot{\mathbf{d}}\}$$

$$+ \{\delta \mathbf{d}\}^T \lambda \frac{EI}{L^3}\int_0^{h_e} \lfloor \mathbf{N} \rfloor^T \lfloor \mathbf{N} \rfloor_{,x} \mathrm{d}x \{\mathbf{d}\} + \{\delta \mathbf{d}\}^T EI \int_0^{h_e} \lfloor \mathbf{N} \rfloor_{,xx}^T \lfloor \mathbf{N} \rfloor_{,xx} \mathrm{d}x \{\mathbf{d}\} = \{\delta \mathbf{d}\}^T \lfloor \mathbf{N} \rfloor^T \{\mathbf{F}_e\} \tag{9}$$

Thus, the element EOM is

$$\frac{1}{\omega_0^2}[m]\{\ddot{\mathbf{d}}\} + \frac{g_a}{\omega_0}[g]\{\dot{\mathbf{d}}\} + (\lambda[a_a] + [K_e])\{\mathbf{d}\} = \{\mathbf{Q}_e\} \tag{10}$$

where the element matrices and load vector are

$$[m] = [g] = \frac{EI}{L^4}\int_0^{h_e} \lfloor \mathbf{N} \rfloor^T \lfloor \mathbf{N} \rfloor \mathrm{d}x$$

$$[a_a] = \frac{EI}{L^3}\int_0^{h_e} \lfloor \mathbf{N} \rfloor^T \lfloor \mathbf{N} \rfloor_{,x} \mathrm{d}x$$

$$[K_e] = EI \int_0^{h_e} \lfloor \mathbf{N} \rfloor_{,xx}^T \lfloor \mathbf{N} \rfloor_{,xx} dx$$

$$\{\mathbf{Q}_e\} = \lfloor \mathbf{N} \rfloor^T \{\mathbf{F}_e\}$$

After assembling, the system EOM becomes

$$\frac{1}{\omega_0^2}[M]\{\ddot{\mathbf{W}}\} + \frac{g_a}{\omega_0}[G]\{\dot{\mathbf{W}}\} + (\lambda[A_a] + [K])\{\mathbf{W}\} = \{\mathbf{Q}\} \tag{11}$$

Solution Procedures

While using frequency domain analysis to determine the critical dynamic pressure for traditional self-excited panel flutter problem, the homogenous form of Eq. (11) is used:

$$\frac{1}{\omega_0^2}[M]\{\ddot{\mathbf{W}}\} + \frac{g_a}{\omega_0}[G]\{\dot{\mathbf{W}}\} + (\lambda[A_a] + [K])\{\mathbf{W}\} = \{\mathbf{0}\} \tag{12}$$

The flutter boundary can be easily turned to be an eigenvalue problem by assuming the response as:

$$\{\mathbf{W}\} = \{\mathbf{\Phi}\} e^{\Omega t} \tag{13}$$

where $\Omega = \alpha + i\omega$ is generally a complex eigenvalue, α and ω are the panel damping rate and frequency, respectively. By substitution of Eq. (13), Eq. (12) leads to a nondimensional eigenvalue problem of the form

$$\kappa[M]\{\mathbf{\Phi}\} = (\lambda[A_a] + [K])\{\mathbf{\Phi}\} \tag{14}$$

where the nondimensional eigenvalue is

$$\kappa = -(\frac{\Omega}{\omega_0})^2 - g_a \frac{\Omega}{\omega_0} \tag{15}$$

This is because that the mass matrix [M] equals to the aerodynamic damping matrix [G] as shown in Eq. (10). While there is no airflow, $\lambda = g_a = 0$, the eigenvalues κ are real and

positive corresponding to the square of natural frequencies of free vibration of traditional panel systems (Model I, IV or V). As λ is increased in value monotonically from zero, the symmetric, real stiffness matrix [K] is then perturbed by the skewed aerodynamic influence matrix $[A_a]$ so that two of the eigenvalues approach each other until they coalesce to the value κ_{cr} at $\lambda = \lambda_{cr}$.

The aforementioned impact problem is not applicable to frequency domain analysis due to the difficulty of describing the boundary condition at the free end (or the impact force). Therefore, simulation of beam time response under airflow and impact force is hopeful to unveil the flutter characteristic of the cantilever beam. The equivalent spring has a stiffness of $k_s = E_sA_s/L_s$ with E_s, A_s, L_s to be the Young's modulus, cross section area and length of the stopper, respectively. Among those popular time integration schemes, the Newmark-β method was adopted here for its stability. The initial conditions used are the first bending mode normalized with $W_{max}/h = 0.1$ and zero initial velocity. Time step length Δt was decided on basis of a bisection strategy: the applied time step size is the one giving slightly different critical dynamic pressure compared to the λ_{cr} attained by its double. The ratio W_{max}/h was checked at each time step for judgement of flutter boundary. The upper limit of W_{max}/h is 4.0, i.e., simulation will be ceased as W_{max}/h equals to or is greater than 4.0. The impact force is

$$F_e = \begin{cases} 0 & W_e > -Gap \\ -k_s(|W_e| - Gap) & W_e \le -Gap \end{cases} \tag{16}$$

where W_e is the transverse deflection at the free end of the beam, *Gap* is the size of the gap marked up in Fig. 2.

RESULTS AND DISCUSSIONS

To validate the finite element model is to compare the results with available analytical analysis results. However, it's found that for the five members in Fig. 3, no analytical flutter boundaries are presented in literature. The alternative way adopted here is to check the flutter boundaries of clamped-clamped beam, and both ends simply supported beam with corresponding analytical results.[6] Figure 4 shows that for these two types of supporting conditions (traditional flutter analysis), finite element analysis agrees well with analytical analysis.

Then, the flutter behavior of a steel beam with dimension L = 1 *in.*(0.0254 *m*), b = 0.1*in.*(0.00254 *m*) and h = 0.006 *in.* (1.524×10^{-4} *m*) was investigated. The beam was discretized with 10 elements. To simulate the tiny gap between the beam free end and stopper top, a gap size of Gap/h = 0.0001 was employed. Computation was carried out for several distributed stiffness values within the range $k_s = 0\sim1.2\times10^6$ *lbf/in.* (2.1×10^8 *N/m*), with the upper limit corresponding to steel beam versus steel stopper case. An aerodynamic damping of $C_a = 0.02$ was assumed and used in the analysis.

Figure 5 is the critical dynamic pressure versus spring stiffness curve of the equivalent spring model II. It shows the existence of an intermediate stiffness ranges roughly from 40 lbf/in.(7005 *N/m*) to 40,000 lbf/in. (7.0×10^6 *N/m*), within which the critical dynamic pressures are over 300. The right and left sides adjacent

to this range are low flutter boundary area having nearly same critical dynamic pressure level as that of the cantilever beam (Fig.6). The time response, force history of representative points A(k_s=0.4, λ=140), B (k_s=2,000, λ=300), C(k_s=2,000, λ=323), D(k_s=200,000, λ=138), E(k_s=0.4, λ=160), F(k_s=200,000, λ=150) are shown in Fig.

7~Fig.11, respectively. Stable time response has a decaying or limit cycle oscillation response history (Fig. 7(a), Fig. 8(a) and Fig. 10(a)). Oppositely, unstable vibration (flutter) is featured as either gradually divergence (Fig. 9(a)) or abrupt increase of W_{max}/h till the upper limit is reached soon (Fig. 11).

Point A is below the flutter boundary for low spring stiffness area. Therefore, as shown in Fig. 7(a), the time response is stable. The spring is so soft that the stopper has little effect on the vibrating beam. Thus the critical dynamic pressure is very near that of the cantilever beam. This can also be verified by the force shape (Fig. 7(d)) of one whole impact. The dominating frequency standing out in Fig.7 (b) is obviously close to the coalescence frequency of cantilever beam as can be identified from Fig. 6 approximately. While the stiffness increased to the intermediate stiffness area, the rebounce phenomenon denoted by the force shapes in both Fig. 8 (d) and Fig. 9 (d) complicated the impact process. Both the stable motion (Point B) and unstable motion (Point C) are dominated by several modes, instead of the coalescence frequency, as shown in Fig. 8 (b) and Fig. 9 (b). However, it's found that the stiffer the spring stopper, the fewer the rebounce. Point D is very close to the flutter boundary of k_s = 200,000, which is λ_{cr} = 139. Comparing the response Power Spectrum Density plots shown in Fig. 10(b) and Fig. 7(b), they have very similar dominating frequency and shape. So the critical dynamic pressure of point D should be close to that of low spring stiffness case. The beat phenomenon observed from Fig. 10 (a) and (b) implies the lowest two modes are about to coalesce.

Figure 3 listed a family of left end clamped beams with ascending stopper stiffness. Among these five types of beam, the flutter boundaries of cantilever beam (model I), connected spring stopper beam (model IV) and right end simply supported beam (model

V) can be determined by frequency domain analysis. The results are shown in Fig. 6, Fig. 12 and Fig. 13, respectively.

The other two models, spring stopper beam and bar stopper beam, are inapplicable to frequency domain analysis. The bar stopper beam model is more alike the seal of X-33 TPS panel. The analysis of this model will help with understanding of the right-hand side of the curve in Fig. 5, time domain analysis of it was also executed. The 0.25 *in.*(0.00635m) long bar stopper has a section area of 0.1×0.1 $in.^2$ (6.451×10^{-6} m^2) and is modeled with 5 bar elements without damping (structural damping will effect the critical dynamic pressure slightly). Learning of stopper material properties turns to be necessary. Similarly, the Newmark-β method was used as time integration scheme. Results from analyses of three types of stopper material are listed in Table 1 to show the trend of flutter boundary variation. Obviously, the drop of critical dynamic pressure as stiffness increased to very stiff is confirmed.

Table 1 Critical dynamic pressure of bar stopper beam with the stopper modeled as bar elements

Stopper Material	Boron	Aluminum	Steel
Density(lb/in^3)	0.083	0.098	0.283
Young's Modulus E_s (msi)	0.0638	8.99	30.2
Equivalent Spring Stiffness $k_s=E_sA_s/L_s$ (lbf/in)	2.55×10^4	3.596×10^5	1.2×10^6
Critical Dynamic Pressure λ_{cr}	322	140	137

Now that the flutter boundaries of all five member beams have been studied, the law beyond them loomed. The cantilever beam with λ_{cr} =136 is both the down and up limit cases of the clamped-spring stopper beam. The clamped-simply supported beam with λ_{cr} = 480 is the upper limit case of the connected spring stopper beam. This can be observed from the right-hand end of the curve in Fig. 12. Both the spring stopper beam and connected spring stopper beam exert constrain to the free end of the cantilever beam. So they will enhance the flutter boundary due to stiffening of the whole dynamic system. It's verified by the appearance of look-like ascending stages appeared in both Fig. 5 and Fig. 12. But the constrain from spring stopper is unidirectional, so spring stopper beam is weaker than connected spring stopper beam which applies a bidirectional constrain to the beam. The descending of flutter boundary is then reasonable. Analysis of bar stopper beam proved this issue.

In summary, the flutter boundary curve shown in Fig. 5 exposed the character of the original impact problem. The time domain analysis procedure was proved to be valid for flutter analysis of systems with impact boundary conditions. However, it seems current work accomplished only the prelude of a systematic work, since the practical problem has inevitable effects from temperature, structural damping, etc.. While the model is expanded to 3D plate and composite materials are considered, predictably, flow direction effect needs attention.

REFERENCES

1. E. H. Dowell, "Panel Flutter: Review of the Aeroelastic Stability of Plates and Shells", *AIAA Journal* , Vol. 8, 1970, pp. 385-399.
2. C. Mei, K. Abdel-Motagaly and R. Chen, "A Review of Nonlinear Panel Flutter at Supersonic and Hypersonic Speeds", *Applied Mechanics Reviews*, Vol. 52, No. 10, 1999, pp. 321-332.
3. R. C. Zhou, D. Y. Xue, and C. Mei, "Finite Element Time Domain-Modal Formulation for Nonlinear Flutter of Composite Panels", *AIAA Journal*, Vol. 32, 1994, pp. 2044-2052.
4. M. L. Blosser, "Development of Metallic Thermal Protection Systems for the Reusable Launch Vehicle", *NASA Technical Memorandum* 110296, Oct. 1996.
5. C. Toulemonde, "Periodic Behavior of Impact Oscillators: Single Degree of Freedom and Multiple Degree of Freedom systems, Experiment", *Proceeding of 1996 EUROMECH-2nd European Nonlinear Oscillation Conference*, Prague, pp.471-474. European Conference Publications, P. O. Box 806, Cambridge CB4 4RT, United Kingdom.
6. J. C. Houbolt, "A Study of Several Aerothermo- elastic Problems of Aircraft Structures in High-Speed Flight", *Ph. D. Thesis, Eidenössischen Technischen Hochschule, The Swiss Federal Institute of Technology,* Zurich, Switzerland, 1958.

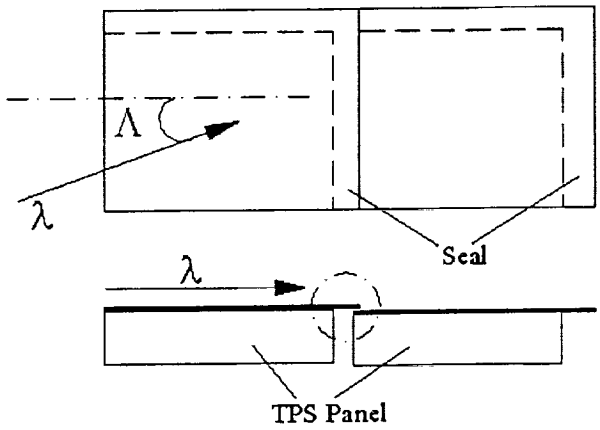

Fig. 1 TPS panel configuration

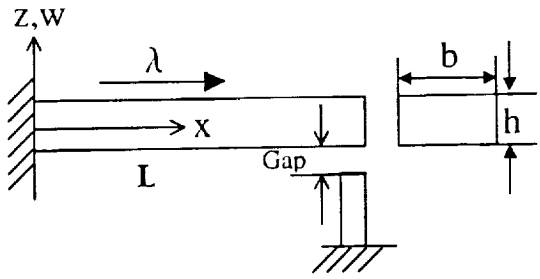

Fig. 2 Cantilever beam with stopper

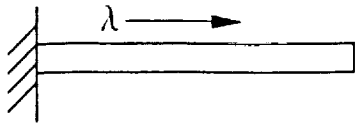

I *Free*

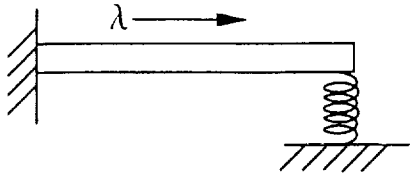

II *Spring Stopper (nonlinear system)*

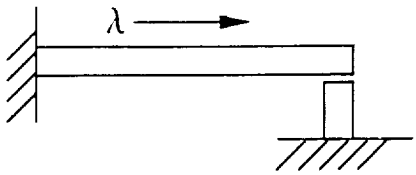

III *Bar Stopper (nonlinear system)*

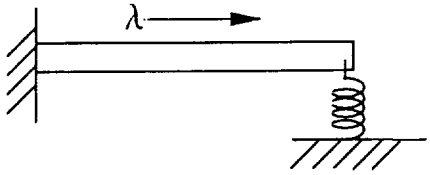

IV *Connected Spring Stopper*

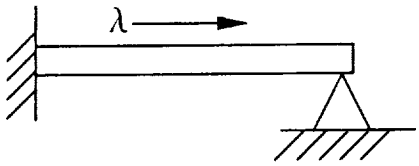

V *Simply Supported*

Fig. 3 Various support conditions at the right end

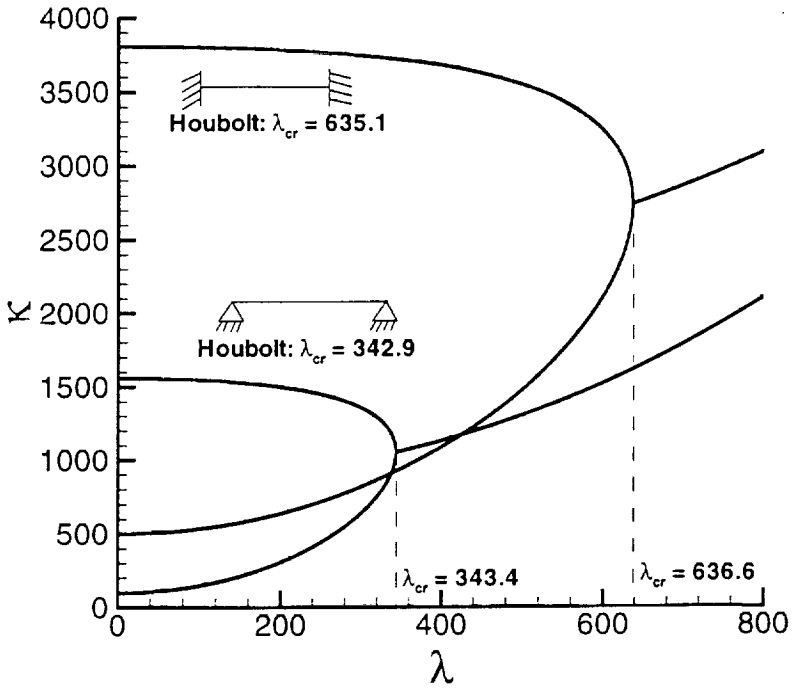

Fig. 4 Critical dynamic pressures: analytical method vs finite element analysis

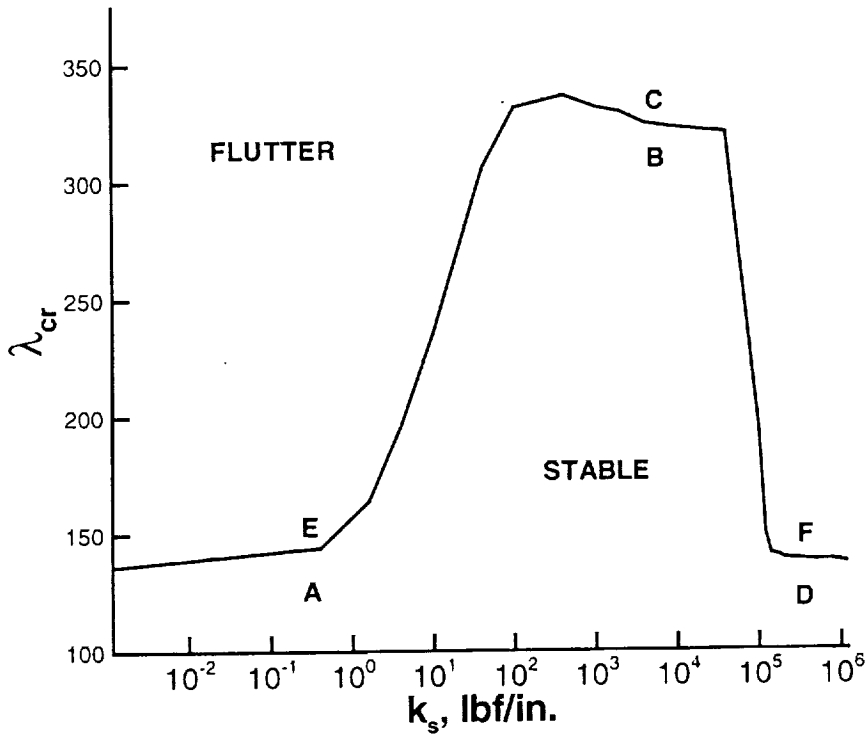

Fig. 5 Flutter boundary of clamped-spring stopper beam

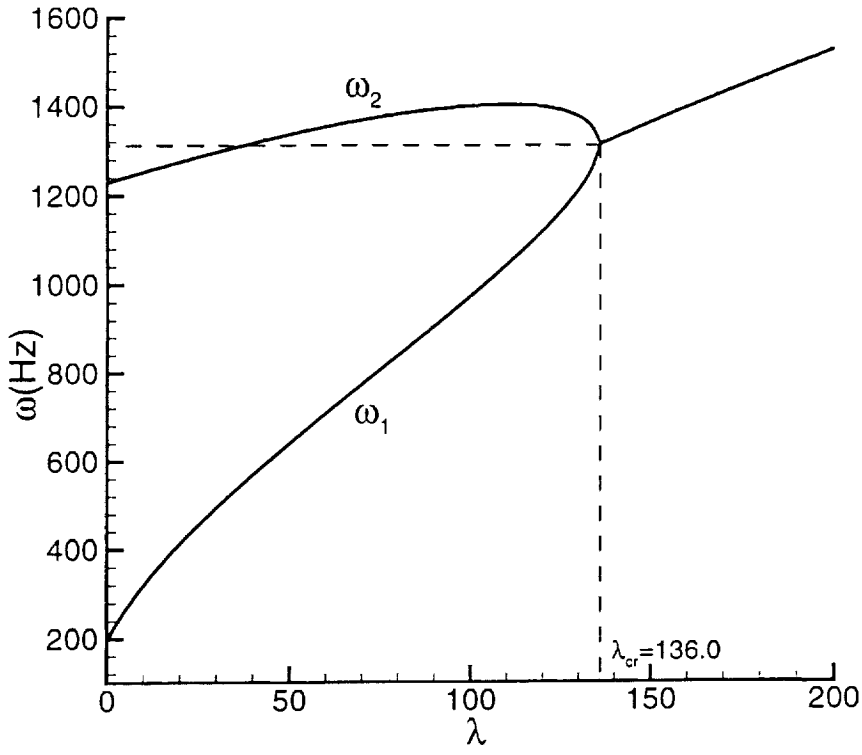

Fig. 6 Cantilever beam critical dynamic pressure

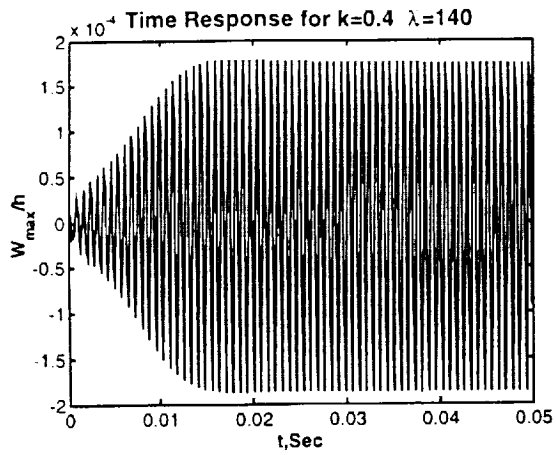

(a)

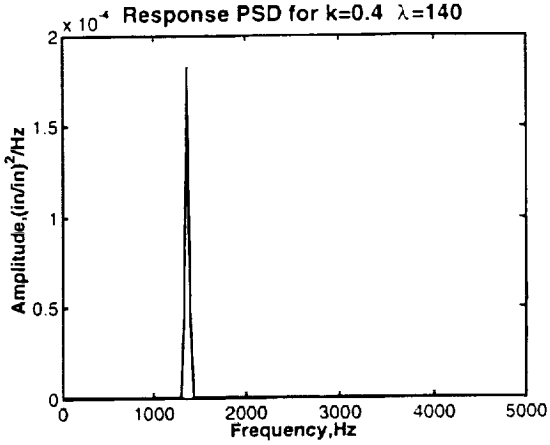

(b)

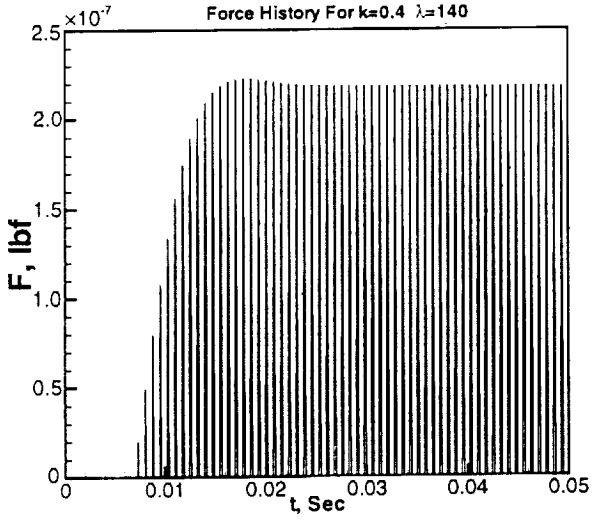

(c)

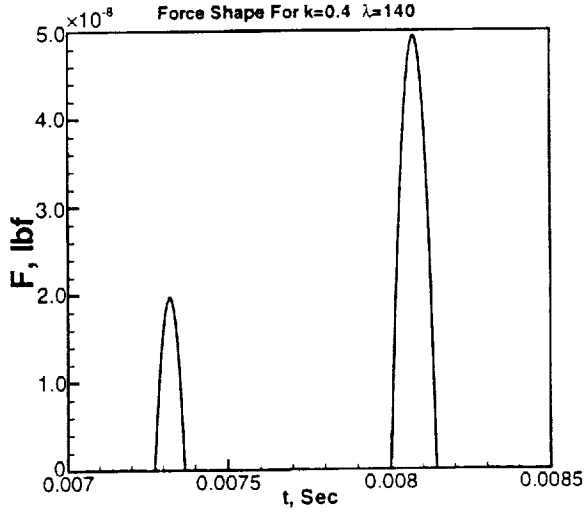

(d)

Fig. 7 Response & force characteristics of point A (k=0.4 λ=140)

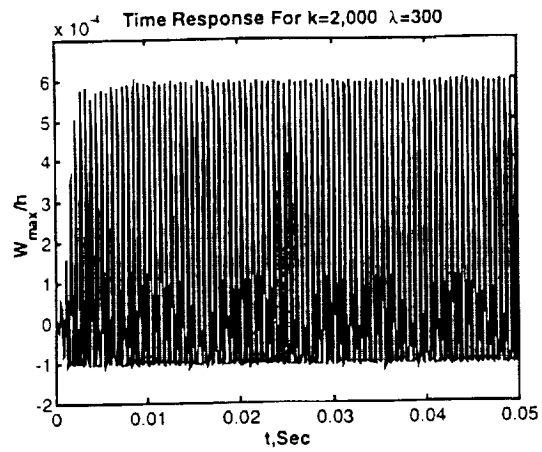

(a)

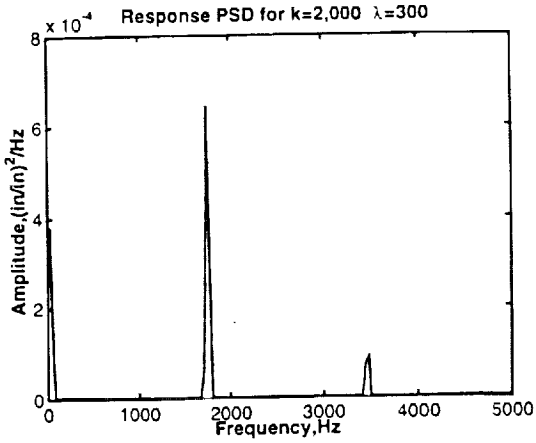

(b)

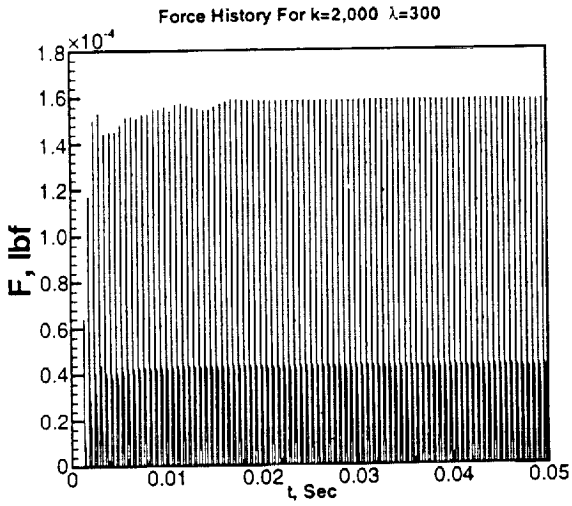

(c)

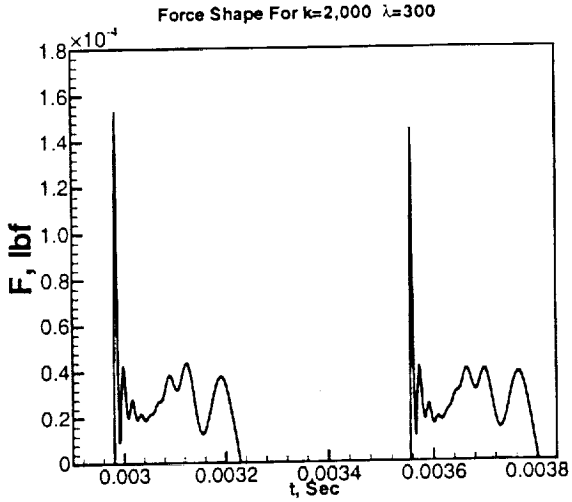

(d)

Fig.8 Response & force characteristics of point B(k=2,000 λ=300)

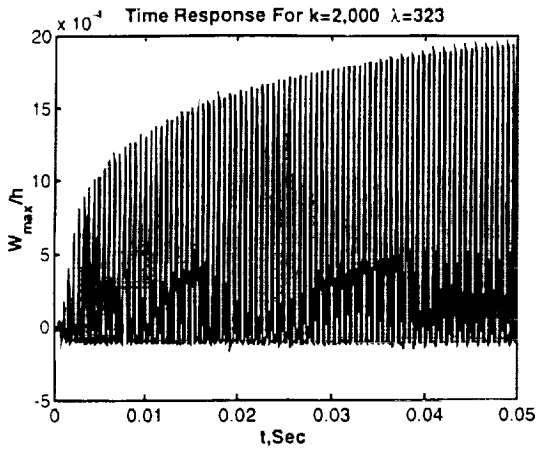

(a)

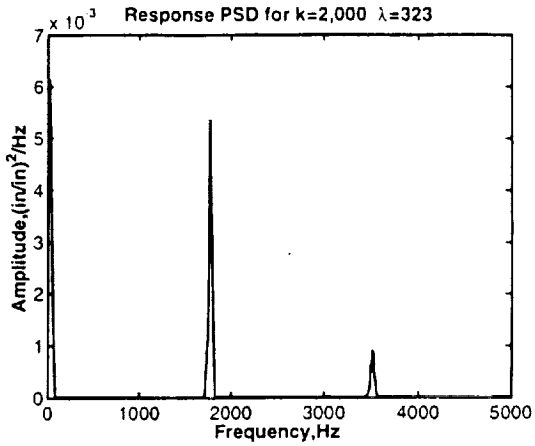

(b)

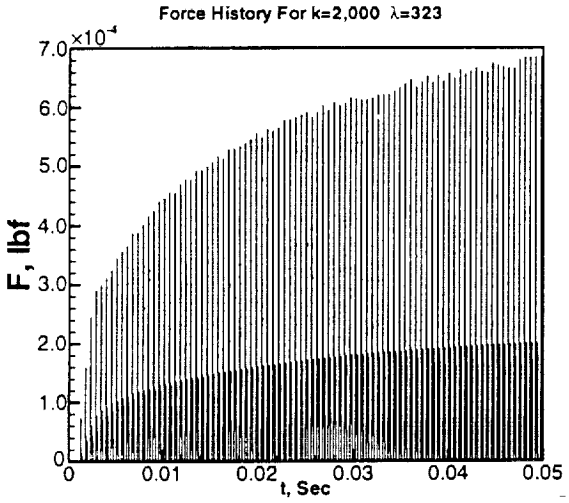

(c)

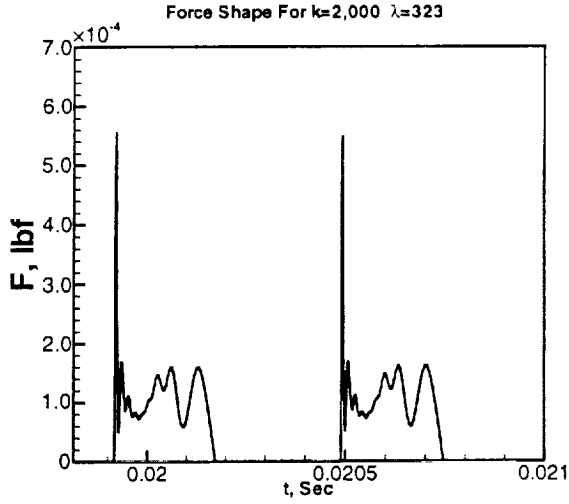

(d)

Fig. 9 Response & force characteristics of point C(k=2,000 λ=323)

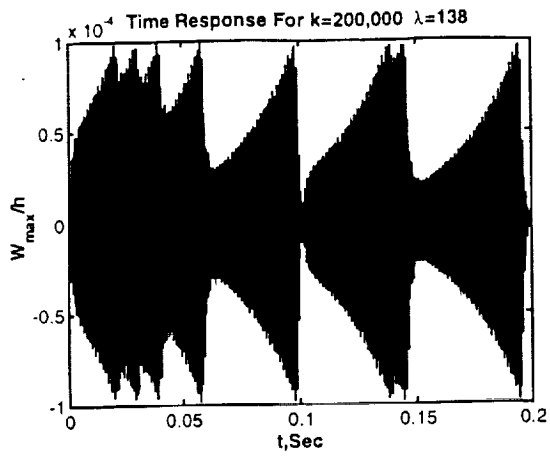

(a)

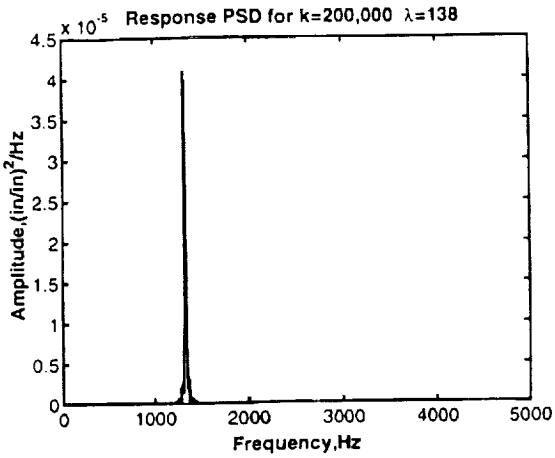

(b)

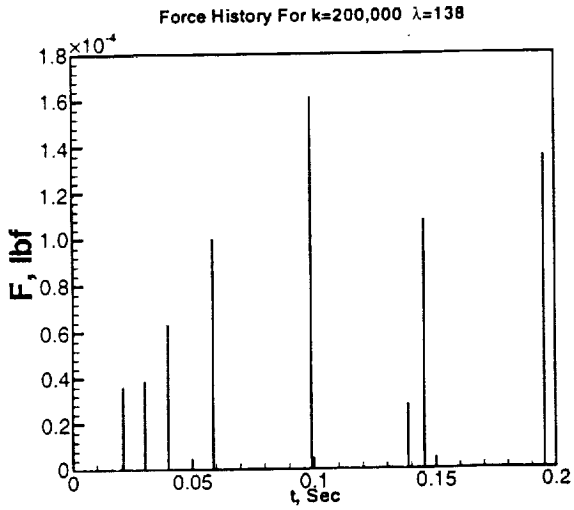

(c)

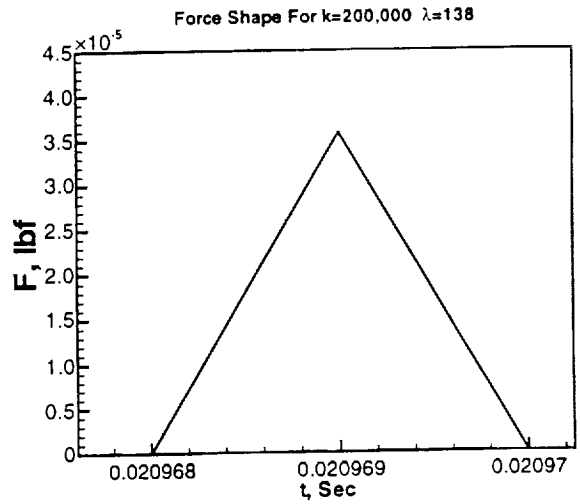

(d)

Fig. 10 Response & force characteristics of point D(k=200,000 λ=138)

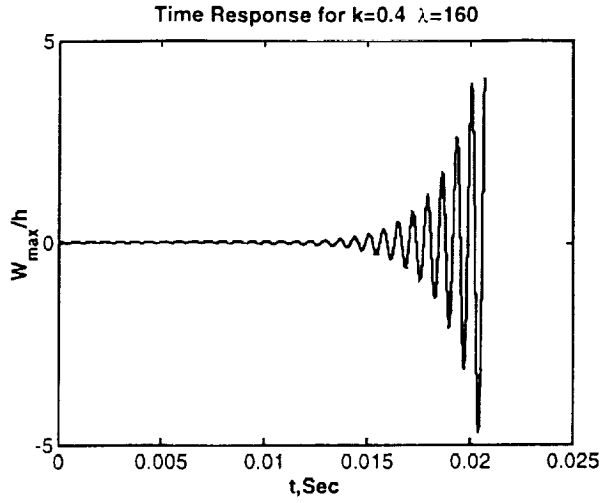

(a)

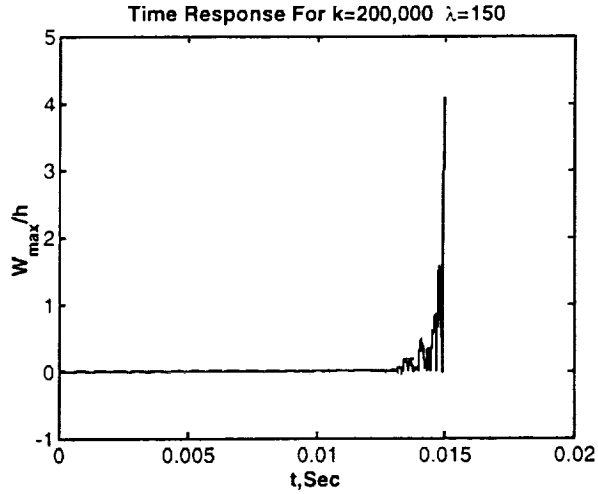

(b)

Fig. 11 Time response for point E(a) and point F(b)

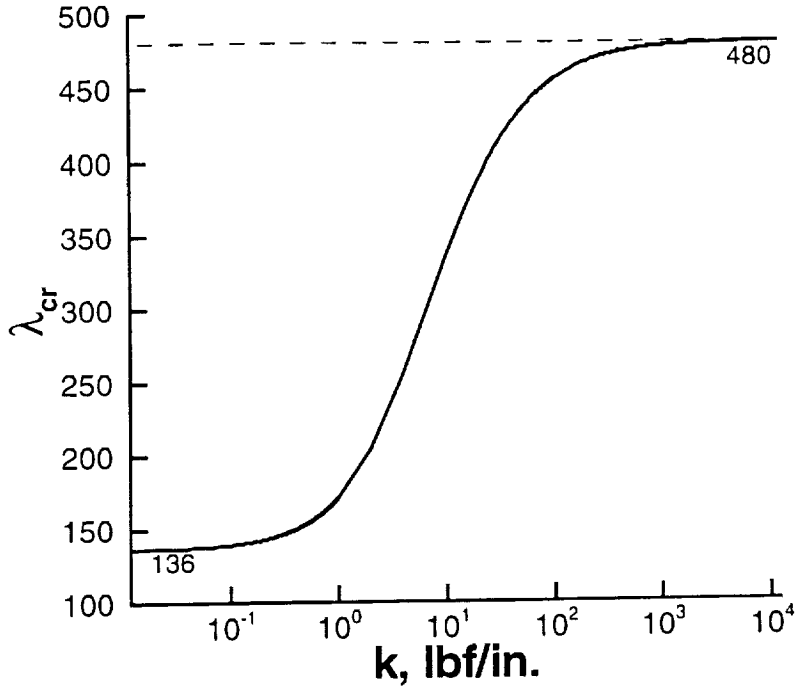

Fig. 12 Flutter boundary of clamped-connected spring beam

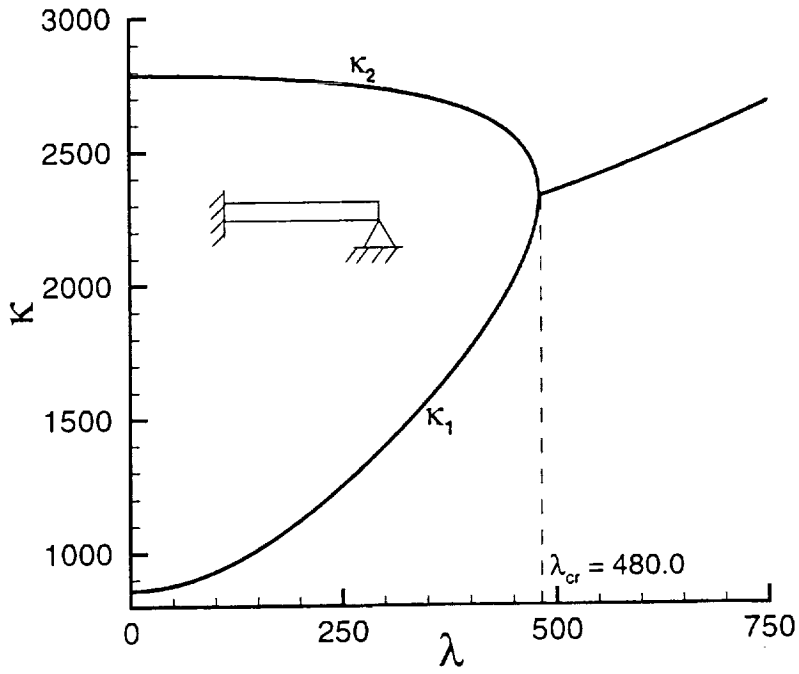

Fig. 13 Critical dynamic pressure of clamped-simply supported beam